High Vapor Pressure Perfluorocarbons Cause Vesicle Fusion and Changes in Membrane Packing

Berenice Venegas,* Marla R. Wolfson,† Peter H. Cooke,‡ and Parkson Lee-Gau Chong*
*Department of Biochemistry and †Department of Physiology and Department of Pediatrics, Temple University School of Medicine, Philadelphia, Pennsylvania 19140; and ‡Eastern Regional Research Center, United States Department of Agriculture, Wyndmoor, Pennsylvania 19038

ABSTRACT Perfluorocarbons (PFCs) hold great promise for biomedical applications. However, relatively little is known about the impact of these chemicals on membranes. We used unilamellar vesicles to explore the effects of PFCs on membrane packing and vesicle stability. Four clinically relevant PFCs with varying vapor pressures (PP1, 294 mbar; PP2, 141 mbar; PP4, 9.6 mbar; and PP9, 2.9 mbar) were examined. Microscopy imaging and spectroscopic measurements suggest that PFCs, especially those with high vapor pressures, lead to vesicle fusion within hours. Upon exposure to PP1 and PP2 for 72 h, vesicles retained a spherical shape, but the size changed from ~200 nm to ~20–40 μm. In addition, membrane packing underwent marked changes during this timeframe. A significant decrease in water content in the lipid polar headgroup regions occurred during the first 1–2-h exposure to PFCs, followed by a steady increase in water content over time. Possible mechanisms were proposed to explain these dramatic structural changes. The finding that chemically inert PFCs exhibited fusogenic activity and marked changes in membrane surface packing is novel, and should be considered when using PFCs for biomedical applications.

INTRODUCTION

Perfluorocarbons (PFCs) are a group of synthetic, chemically inert, water-immiscible compounds. They are composed mainly of C and F, and the C-F bond is highly stable (1). Humans lack the enzymes required to cleave the C-F bond. Within this context, PFCs are considered biologically inert. Animal and clinical studies showed that PFCs are also physiologically compatible.

Perfluorocarbons have many other unique properties that lend great promise for biomedical applications. Perfluorocarbons dissipate heat and acoustical stress, and may prevent carbonization of bone (2). They also have low surface tension. This characteristic serves to stabilize the surfactant-deficient lung by reducing the amount of pressure required to inflate the lung. In addition, because PFC liquids are incompressible, they prevent the lung from completely collapsing during expiration. These liquids also have high solubility of respiratory gases, and work as an excellent transporter or exchanger for oxygen and carbon dioxide. By filling the lungs with PFCs, oxygen can be delivered to the lungs to treat severe respiratory disease (2–4). Clinical studies of neonates and young children showed that PFC-based liquid ventilation improves oxygenation and lung function (5). Based on the same oxygen-transporting phenomenon, PFC emulsions were used as blood substitutes (6–8). Perfluorocarbons may also be used to deliver pulmonary drugs (5,9), and to function as imaging contrast agents (10–12). Preclinical studies also showed that PFC vapor and neat liquids reduce inflammation and mitigate damage in the lung (13,14).

Perfluorocarbon molecules are primarily uncharged, lipophilic entities. When they enter a cell, they must first associate with lipid bilayers in cell membranes (6). In vitro studies demonstrated that cellular effects of PFCs correlate with their lipid solubility (15). Thus, the most logical and fundamental study to understand fully PFCs in cells or tissues would involve a thorough investigation of interactions of PFCs with lipid membranes. However, very few studies have been performed to reveal the biophysical details and principles underlying PFC-membrane interactions. The NMR work of Ellena et al. (16) demonstrated that perfluorooctyl bromide (PFOB) has limited lipid solubility in 1-palmitoyl-2-oleoyl-L-α-phosphatidylcholine (POPC) bilayers, but inside the bilayer, PFOB resides in the bilayer center (midplane region), with its long axis aligned perpendicular to the membrane normal. Perhaps because of this rather unusual disposition, PFOB does not produce any significant changes in either acyl chain or headgroup structure (16). Gerber et al. (17) reported that PFOB fluidizes a dipalmitoyl-L-α-phosphatidylcholine (DPPC) monolayer. Although these studies are interesting, little is known about the effects of PFCs on membrane lateral organization, bilayer packing, membrane morphology, and the temporal evolution of those effects. Furthermore, PFOB has a low vapor pressure (14.6 mbar) (17). The findings from PFOB may not apply to PFCs with high vapor pressures (for examples, see below).

Here, we used unilamellar vesicles, composed of either POPC or cholesterol plus POPC, to explore the effects of PFCs on membrane packing and vesicle stability. Four clinically relevant PFCs, i.e., perfluoro-2-methylpentane (PP1, 294 mbar), perfluoromethylcyclohexane (PP2, 141 mbar),

Submitted March 13, 2008, and accepted for publication August 5, 2008.

Address reprint requests to Parkson Lee-Gau Chong, Dept. of Biochemistry, Temple University School of Medicine, 3420 N. Broad St., Philadelphia, PA 19140. Tel.: 215-707-4182; Fax: 215-707-7536; E-mail: pchong02@temple.edu.

Editor: Paul H. Axelsen.

0006-3495/08/11/4737/11 $2.00

doi: 10.1529/biophysj.108.133496

perfluoro-1,3,5-trimethylcyclohexane (PP4, 9.6 mbar), and perfluoromethyldecalin (PP9, 2.9 mbar), were used (Fig. 1). These PFCs exhibit a range of physicochemical properties (e.g., vapor pressure), and were used in vivo for respiratory applications. The oxygen gas solubility of these PFCs is within a narrow range, and is thus unlikely to contribute a marked confounding experimental influence. The vapor pressures of PFCs are strongly correlated with the reduced production of inflammatory mediators and increased lung compliance (14,18). Our data from photon correlation spectroscopy, energy transfer-based lipid mixing assays, and phase-contrast and electron microscopy suggest that PFCs, especially those with high vapor pressures, lead to vesicle aggregation/fusion on the timescale of hours. During this time period, membrane packing, as revealed by the generalized polarization (GP) of Laurdan (6-lauroyl-2-(dimethylamino)-naphthalene) fluorescence, also undergoes marked changes. Possible mechanisms are proposed to explain these dramatic structural changes.

MATERIALS AND METHODS

Materials

We obtained POPC and cholesterol from Avanti Polar Lipids (Alabaster, AL). We obtained 6-lauroyl-2-(dimethylamino)naphthalene (Laurdan), *N*-(7-nitrobenz-2-oxa-1,3-diazol-4-yl)-1,2-dihexadecanoyl-*sn*-glycero-3-phosphoethanolamine, triethylammonium salt (NBD-PE), and lissamine rhodamine B 1,2-dihexadecanoyl-*sn*-glycero-3-phosphoethanolamine triethylammonium salt (rhodamine-DHPE) from Invitrogen-Molecular Probes (Eugene, OR). We purchased PP1, PP2, PP4, and PP9 from F2 Chemicals (Lancashire, UK). The PFCs were stored at room temperature in a well-sealed vial.

Vesicle formation

Large unilamellar vesicles (LUVs), composed of either POPC or POPC plus cholesterol (molar ratio, 7:3), were produced by the extrusion method (19). Briefly, POPC and cholesterol dissolved in chloroform were combined in the appropriate proportions in a round-bottomed culture tube. Chloroform was evaporated by a stream of nitrogen gas, and further dried under high vacuum (~100–200 millitorr), for more than 12 h. Then, we added 50 mM Tris buffer containing 10 mM EDTA and 0.02% NaN_3 (pH 7.2), prewarmed at 40°C, to the dry lipid film. The tube was then flushed with argon and capped, followed by vortexing at ~40°C, until all the lipids were dispersed into the aqueous phase. After incubation at room temperature overnight, the lipid dispersions were extruded (Lipex Biomembranes, Vancouver, British Columbia, Canada) at 40°C 10 times through two stacked 200-nm Nucleopore polycarbonate filters (Whatman, Florham Park, NJ) under nitrogen gas pressure to form LUVs. After extrusion, vesicles had a typical size of 175–190 nm in diameter. The LUVs were then flushed with argon and stored in a desiccator under vacuum to prevent lipid oxidation (20) before use. For energy-transfer experiments, vesicles were prepared in the same manner, except that the molar ratio of membrane constituents was changed to 69:30:1 for POPC/cholesterol/NBD-PE (or rhodamine-DHPE) mixtures.

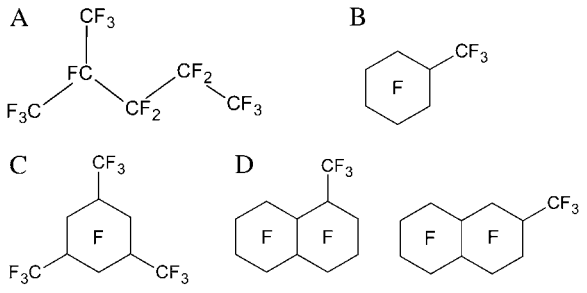

FIGURE 1 Molecular structures of PFCs used in this study. (*A*) Perfluoro-2-methylpentane (PP1). (*B*) Perfluoromethylcyclohexane (PP2). (*C*) Perfluoro-1,3,5-trimethylcyclohexane (PP4). (*D*) Perfluoromethyldecalin, mixture of several isomers (PP9).

Incubation of vesicles with PFCs

Vesicles were diluted to a lipid concentration of 300 μM and incubated with PFC (5%, v/v) at room temperature. The final volume of lipid vesicles plus PFC was 5 mL. The mixture was placed in a 20-mL vial, which was hermetically sealed. The sample underwent gentle agitation over the entire length of the experiment. Experiments were performed in triplicate for statistical purposes. Because the PFCs used are dense and water-immiscible liquids, the presence of PFCs should not have affected the concentration of lipid vesicles in the sample. The control was made of the same vesicles in the absence of PFCs.

Laurdan generalized polarization

Laurdan is an environmentally sensitive fluorescent probe. The generalized polarization (GP) of Laurdan fluorescence is defined as $GP = (I_{435} - I_{500})/(I_{435} + I_{500})$, where I_{435} and I_{500} are the fluorescence intensities of Laurdan at 435 and 500 nm, respectively. The GP reflects membrane packing in the polar-nonpolar interfacial regions (21), where the chromophore of Laurdan resides (22,23). Higher GP values indicate tighter membrane packing. The concentration of Laurdan stock solution in dimethylsulfoxide (DMSO) was determined photometrically at 364 nm, using the extinction coefficient ε equal to 20,000 $cm^{-1}M^{-1}$ (in methanol).

Laurdan in DMSO was added to the lipid vesicles ([POPC] = 300 μM) in a probe/lipid molar ratio of 1:200. The mixture was incubated overnight under argon and protected from light. The amount of DMSO added to the sample was always <1% (v/v); this amount of DMSO was previously shown not to perturb membrane structure to any significant extent (24). Then PFC was added, and the vial was sealed. At each time point, 200 μL were taken from the sample vial through a valve, such that the pressure generated by the PFC vapor in the sample vial remained constant throughout the entire experiment. The aliquot that was removed was added to a fluorescence cuvette containing 1.6 mL of Tris buffer. The emission spectrum of Laurdan was recorded from 400–520 nm, with excitation wavelength set at 340 nm on an ISS K2 fluorometer (ISS, Champaign, IL).

Particle size and size distribution as determined by dynamic light scattering

The hydrodynamic diameters of vesicles were measured at 25°C by photon correlation spectroscopy, using a Malvern Zetasizer 1000HAS spectrometer (Malvern Instruments, Wores, UK). The light source was a 10-mW He-Ne laser (633 nm), and the scattered light was measured at a right angle, using an avalanche photodiode detector. Because very dilute solutions were used, the values for the refractive index and viscosity were set equal to the values of water for the calculations of hydrodynamic diameters. Specifically, the refractive index was 1.33 for all samples examined, and the viscosity was 0.891 cP at 25°C (in accordance with the Handbook of Chemistry and Physics, 68th ed.). The data were analyzed using the Contin algorithm (provided by Malvern Instruments), which calculates the *Z*-average size and polydispersity. The *Z*-average size is the average hydrodynamic diameter of the vesi-

cles, whereas polydispersity is a measure of the width of the vesicle size distribution.

Energy transfer between NBD-PE and rhodamine-DHPE: a lipid-mixing assay

Concentrations of stock solutions of NBD-PE and rhodamine-DHPE dissolved in chloroform were determined photometrically, using the extinction coefficients $\varepsilon_{\text{NBD-PE}} = 21{,}000\ \text{cm}^{-1}\text{M}^{-1}$ (in methanol at 463 nm), and $\varepsilon_{\text{rhodamine-DHPE}} = 75{,}000\ \text{cm}^{-1}\text{M}^{-1}$ (in methanol at 560 nm). The LUVs (~200 nm in diameter), composed of POPC/cholesterol/NBD-PE or POPC/cholesterol/rhodamine-DHPE (molar ratio, 69:30:1), were prepared as described earlier.

An equimolar mixture of POPC/cholesterol/NBD-PE and POPC/cholesterol/rhodamine-DHPE LUVs (150 μM total lipid in each population) was incubated with PFC, as described earlier. At each time point, 200 μL were removed from the sample vial through a valve. The aliquot was added to a cuvette containing 1.6 mL of Tris buffer for fluorescence readings. The emission spectrum was recorded from 500–620 nm on an SLM 8000C fluorometer (SLM Instruments, Urbana, IL), with an excitation wavelength set at 450 nm. The emission spectrum should exhibit two peaks: one is centered at 530 nm because of the emission of NBD-PE, and the other appears at ~585 nm, corresponding to the emission from rhodamine-DHPE.

The resonance energy transfer between NBD-PE (donor) and rhodamine-DHPE (acceptor) can occur if these two probes are in close proximity because of lipid mixing between these two vesicle populations. Lipid-mixing can occur through vesicle coalescence or vesicle fusion. As a result of lipid mixing, the peak intensity at 585 nm, relative to that at 530, was enhanced. The extent of energy transfer is reflected by the parameter $E = (I_{\text{NBD}} - I_{\text{Rhod}})/(I_{\text{NBD}} + I_{\text{Rhod}})$, where I_{NBD} and I_{Rhod} are the fluorescence intensities at 530 nm and 585 nm, respectively. The limiting value of E ranges between 1 and -1, corresponding to 0 and 100% energy transfer, respectively. A more negative E value indicates more energy transfer and more lipid-mixing.

Electron and phase contrast microscopy

The effects of PFCs on the morphology and aggregation state of lipid vesicles were examined by negative staining-transmission electron microscopy (EM) and phase-contrast microscopy. The sample for negative-staining EM was prepared as described (25). Briefly, 10-μL aliquots of 0.10% (w/v) of a poly-L-lysine solution (in water) were placed on carbon-coated 400-mesh Cu grids. Excess volume was removed by adsorption with Whatman No. 2 filter paper at the edge of the grid, and the remaining poly-L-lysine solution was allowed to dry for 10 min on the grid before the addition of sample; 10 μl aliquots of sample were added to the poly-L-lysine-coated Cu grids for 5 s, and washed with a controlled stream of 5–6 drops of 2% uranyl acetate stain (pH 4.8). The grid was then air-dried for 5 min before loading into the microscope. Negatively stained areas of samples were examined by bright-field transmission EM at an accelerating voltage of 80 kV in a Philips CM12 cryo-version scanning-transmission electron microscope (FEI Co., Inc., Hillsboro, OR). For phase-contrast microscopy, an inverted optical microscope (Model IRBE, Leica Microsystems, Bannockburn, IL), equipped with phase-contrast lenses and a halogen lamp house, was used.

RESULTS

Fig. 2 shows the effects of PFCs on the average diameter and polydispersity of vesicle particles composed of cholesterol (30 mol %) and POPC (70 mol %) at room temperature. In the presence of PP1 and PP2 (high vapor pressure PFCs; Fig. 1), both the particle size and size distribution (polydispersity) increased abruptly with time during phases I (time = 0–2 h) and II (time = 2–8 h) (Fig. 2). In phase III (time = 8–120 h), the size and size distribution increased with time much less dramatically, and approached a plateau near the end of the experiment (Fig. 2). Low vapor pressure PFCs (PP4 and PP9; Fig. 1) produced a much smaller and slower increase in particle size and size distribution over time. The timescale for PFC-induced particle size change was consistent with the report that PFC uptake into cell membranes is relatively slow and takes several hours to reach equilibrium (26). During this experimental time period (0–120 h), the control (the same vesicles in the absence of PFCs) showed very little change in size (average diameter, 186.5 ± 15.8 nm) and size distribution (polydispersity, 0.076 ± 0.031). To rule out the emulsification of PFCs in the aqueous solution, we mixed PP1, PP2, PP4, and PP9 with Tris buffer, and the mixtures were gently agitated for the same number of hours. For this control, there was no detection of particles by photon correlation

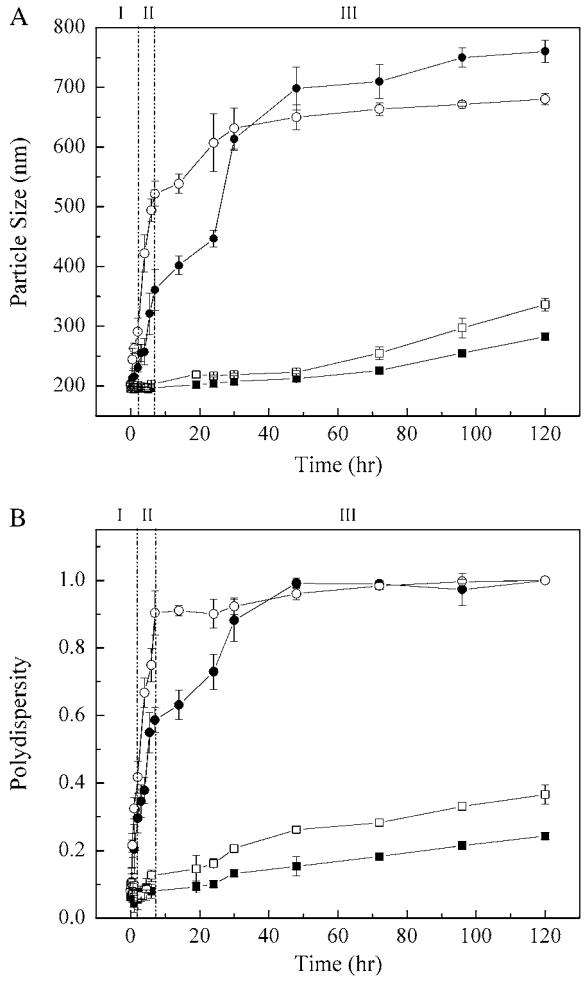

FIGURE 2 Temporal evolution of particle size (*A*) and polydispersity (*B*) in the presence of (●) PP1, (○) PP2, (■) PP4, and (□) PP9, in liposomes composed of POPC (70 mol %)and cholesterol (30 mol %). Control (vesicles in absence of PFCs): vesicle size = 186.5 ± 15.8 nm, and polydispersity = 0.076 ± 0.031, over time period of 120 h. Three different stages described in text are indicated by I, II, and III.

spectroscopy, suggesting that the dramatic increase in particle size and size distribution seen in Fig. 2 was attributable to direct interaction between PFCs and lipid membranes.

Fig. 3 shows that high vapor pressure PFCs (e.g., PP1 and PP2) can also induce remarkable changes in particle size for POPC LUVs in the absence of cholesterol. However, the rate of particle-size increase for POPC vesicles was significantly slower than that for POPC/cholesterol (30 mol %) (Fig. 3, *inset*). Bilayer membranes of pure POPC are not supposed to possess lipid microdomains. In contrast, sterol superlattice domains exist in POPC/cholesterol (30 mol %) mixtures (27,28).

An additional experiment was designed to test whether the extent of sterol superlattice affects the rate of PFC-induced vesicle aggregation/fusion (Fig. 4). In this experiment, POPC/cholesterol vesicles with three different sterol mole fractions were used. We chose 22.2 mol %, because it is one of the critical sterol mole fractions (C_r) for maximal sterol superlattices (28–30), and used 21.0 and 23.4 mol %, because they are two noncritical mole fractions in the neighborhood of the critical mole fraction 22.2 mol %. As shown in Fig. 4, the particle size increased considerably over time upon exposure to PP1 for vesicles at noncritical sterol mole fractions (e.g., 21.0 and 23.4 mol %), but increased little for vesicles at the critical sterol mole fraction 22.2 mol %. This result (Fig. 4) indicates that the rate of particle-size increase engendered by PP1 depends on the extent of sterol superlattice. This kind of remarkable biphasic change in membrane properties at C_r was described previously (20,27,28).

To understand the origin of the particle-size increase produced by PFCs, an energy-transfer assay was performed

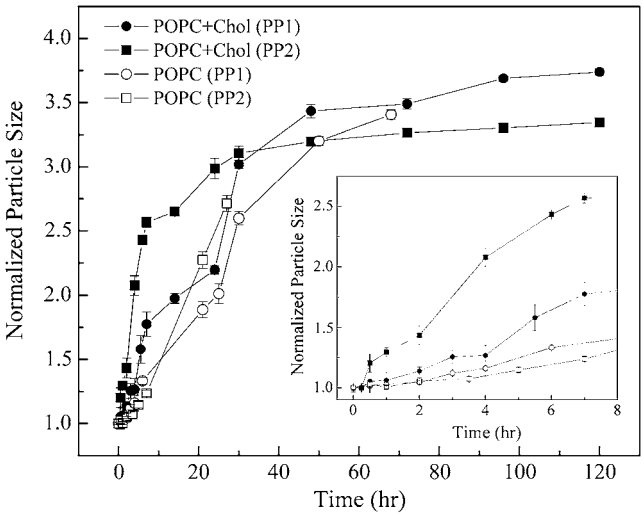

FIGURE 3 Time dependence of particle size of vesicles composed of POPC/cholesterol (30 mol %) (*solid circles* and *squares*) and POPC alone (*open circles* and *squares*) upon exposure to PP1 (*circles*) and PP2 (*squares*). For each sample set, vesicle size at time zero was normalized to one. (*Inset*) Enlarged plot for data points obtained during first 8 h.

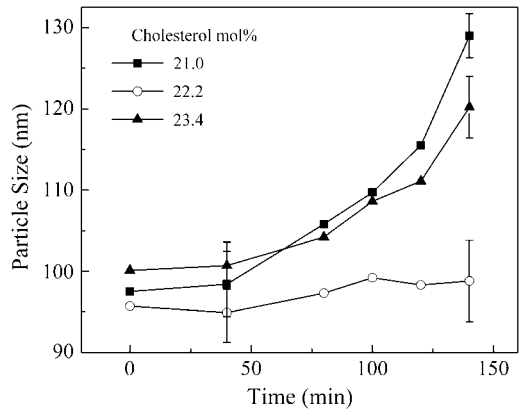

FIGURE 4 Time variation of particle size of vesicles composed of POPC/cholesterol upon exposure to PP1. Experiments were performed using three different cholesterol mole fractions: 21.0 (*solid squares*), 22.2 (*open circles*), and 23.4 (*solid triangles*) mol %; 22.2 mol % is a critical mole fraction (C_r) for centered rectangular superlattices, whereas 21.0 and 23.4 mol % are non-C_r values. [POPC] = 300 μM.

to assess the degree of lipid-mixing between vesicles in the presence of PFCs. Lipid-mixing may result from vesicle fusion, vesicle coalescence, and lipid spontaneous transfer between vesicles. In this experiment, the emission spectrum of an equimolar mixture of vesicles composed of POPC/cholesterol/NBD-PE (molar ratio, 69:30:1) and POPC/cholesterol/rhodamine-DHPE (molar ratio, 69:30:1) was measured as a function of PP1 exposure time (Fig. 5). The peak intensity at 585 nm (because of rhodamine-DHPE), relative to that at 530 nm (because of NBD-PE), increased over time (Fig. 5). From the emission spectra, the extent of lipid-mixing between NBD-PE and rhodamine-DHPE from their originally separated vesicles can be determined in terms of the energy transfer parameter $E = (I_{NBD} - I_{Rhod})/(I_{NBD} + I_{Rhod})$ (as defined in Materials and Methods). Comparing the energy-transfer data in the presence and absence of PP1 (+PP1 and −PP1, respectively, in Fig. 6 *A*), it can be seen that the spontaneous transfer of NBD-PE and rhodamine-DHPE between vesicles contributes no more than 30% of the total lipid-mixing. The E values obtained from samples in the presence of PP1 minus the E values obtained from samples in the absence of PP1 because of spontaneous lipid transfer gives ΔE (labeled as (+PP1)-(−PP1), Fig. 6 *A*, *lower panel*). The ΔE value reflects the PP1-induced energy transfer caused by lipid-mixing attributable to vesicle coalescence or fusion. A more negative value of ΔE means a higher extent of vesicle coalescence or fusion. It is clear from the ΔE data (Fig. 6 *A*, *lower panel*) that PP1 induces a dramatic increase in vesicle coalescence or fusion in the first 5 h of PP1 exposure. This process continues, but at a slower rate, after $t = 5$ h.

The lipid composition in the equimolar mixture of POPC/cholesterol/NBD-PE (molar ratio, 69:30:1) and POPC/cholesterol/rhodamine-DHPE (molar ratio, 69:30:1) is not the same as that in the POPC/cholesterol (molar ratio, 7:3) used in the previous experiment (Fig. 2). Therefore, the effect of

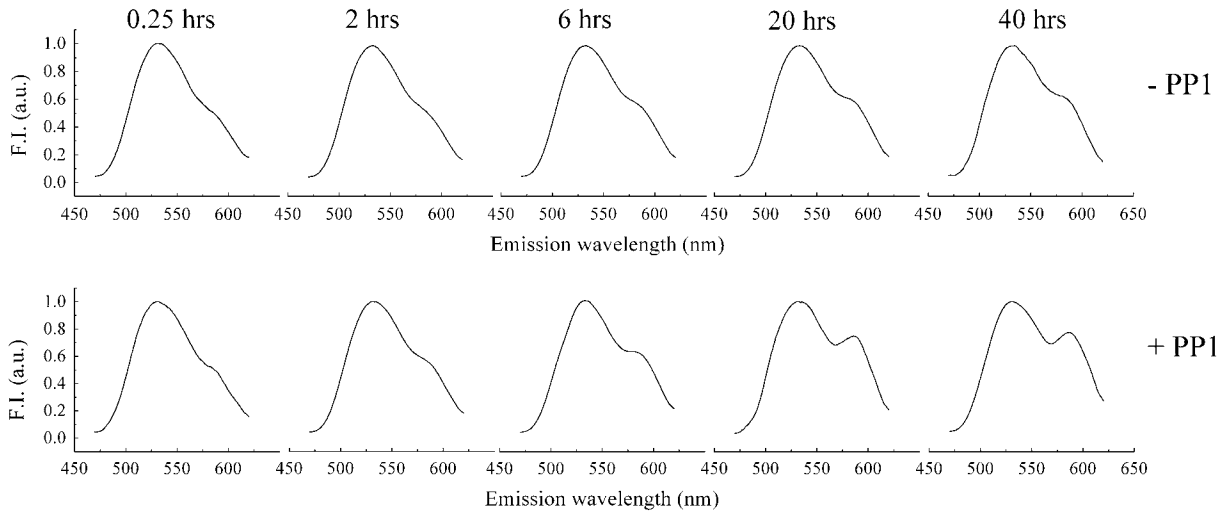

FIGURE 5 Fluorescence emission spectra of an equimolar mixture of two vesicle populations (NBD-PE/POPC/cholesterol and rhodamine-DHPE/POPC/cholesterol) in the absence (−PP1) and presence (+PP1) of PP1 after 0.25, 2, 6, 20, and 40 h of incubation at room temperature under gentle agitation. Excitation was set at 450 nm. Peaks at 525 and 585 nm, measured at room temperature under gentle stirring, correspond to NBD-PE and rhodamine-DHPE emission, respectively. Fluorescence intensity at 525 nm is normalized to unity. The PP1-induced energy transfer from NBD-PE to rhodamine-DHPE is clearly observable at >6 h.

PP1 on particle size in this equimolar mixture was examined. As shown in Fig. 6 *B*, PP1 causes a significant increase in particle size of this equimolar mixture over a time period of 47 h (+PP1, Fig. 6 *B*). In comparison, the same sample in the absence of PP1 (−PP1, Fig. 6 *B*) exhibits much less change in particle size because of spontaneous vesicle aggregation in the same time period (−PP1, Fig. 6 *B*). The net size change ($\Delta size$) attributable to PP1 is expressed as (+PP1)-(−PP1) (Fig. 6 *B*, *lower panel*). It is clear from the $\Delta size$ data that PP1 induces a significant particle-size increase, and that the rate of size increase undergoes an abrupt change at $t = 5$ h. The PP1-induced net increase in particle size ($\Delta size$, Fig. 6 *B*) correlates well (correlation coefficient, 0.9) with the extent of lipid-mixing (ΔE, Fig. 6 *A*). This implies that the PP1-induced and PP2-induced sharp increase in particle size seen in Fig. 2 is likely attributable to lipid-mixing resulting from either vesicle coalescence or vesicle fusion.

The suggestion of vesicle fusion and coalescence is strongly supported by phase-contrast microscopy (Fig. 7) and negative-staining EM (Fig. 8) data. Fig. 7 shows that after exposure to PP1 and PP2 (high vapor pressure PFCs) for 72 h, cholesterol/POPC vesicles (~200 nm originally) become giant spherical vesicles at sizes of 20–40 μm. The spherical shape and large size (Fig. 7) can be explained most likely by multiple vesicle fusion, i.e., fusion involving more than two vesicles (31). Our result shows for the first time, to our knowledge, that high vapor pressure PFCs have strong fusogenic activity with lipid vesicles. In contrast, low vapor pressure PFCs such as PP4 and PP9 produce fewer and much smaller giant vesicles, some of which are aggregated with small vesicles (Fig. 7).

If the giant vesicles observed in Fig. 7 are attributable to vesicle fusion involving multiple vesicles, we might be able to capture EM pictures for prefusion stages, such as vesicle coalescence. Fig. 8 shows that this is probably the case. The EM picture in Fig. 8 shows vesicle coalescence after cholesterol/POPC vesicles were exposed to PP2 for 72 h. It is notable, as seen in Fig. 8, that internal vesicular structures exist inside each of the two opposing vesicles.

As such, the abrupt increase in particle size in region I shown in Fig. 2 can be attributed to vesicle aggregation, followed by immediate vesicle coalescence or vesicle fusion. Vesicle aggregation is a prerequisite of vesicle coalescence and fusion. Vesicle aggregation is known to involve lipid headgroup dehydration and headgroup conformational changes, especially at the sites of vesicle contacts (32). It is then reasonable to predict that membrane packing in the headgroup regions is altered during the time course of PFC exposure. This prediction was tested by Laurdan's GP, which is known to be sensitive to membrane packing in membrane-water interfacial regions (23,33–35).

The effects of PFCs on Laurdan's GP in the cholesterol/POPC (molar ratio, 3:7) vesicles are presented in Fig. 9. In all cases examined, there was an initial increase in GP in region I (~1 or 2 h after exposure to PFCs), followed by a steady decrease in GP over time (Fig. 9, *regions II* and *III*). An increase in GP implies an increase in membrane-packing tightness or less water in the membrane polar headgroup regions (36). A decrease in GP signals a disordering effect on membrane structure (36). It appears from Figs. 2 and 6–9 that membrane packing in the polar headgroup regions is closely related to PFC-induced vesicle aggregation/fusion. The GP value of the control (same Laurdan-containing vesicles in the

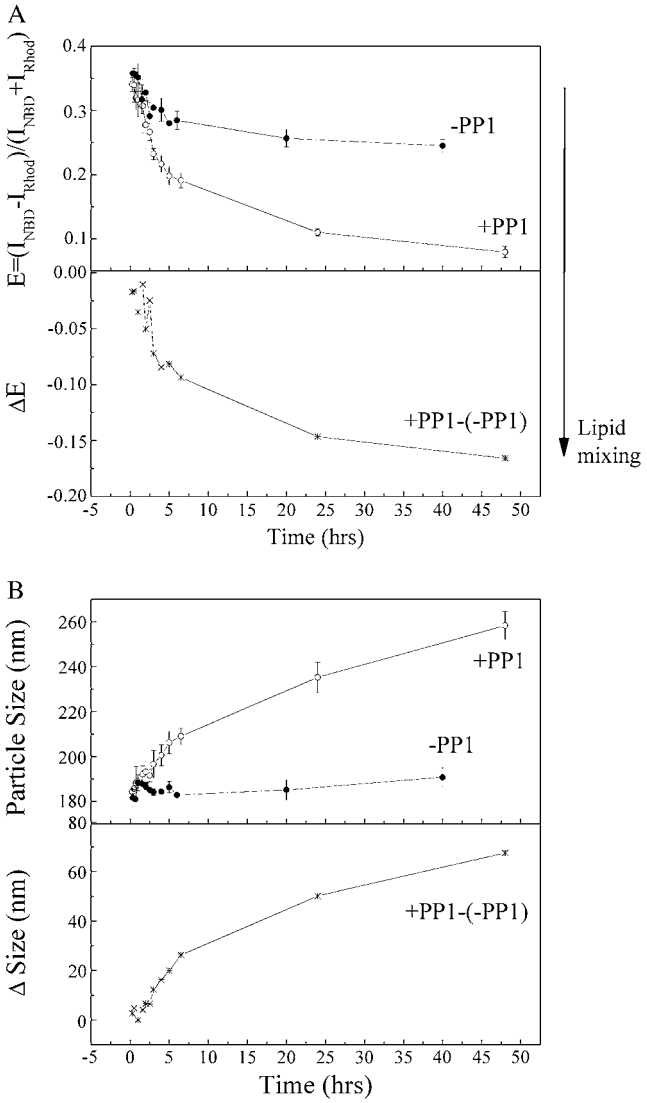

FIGURE 6 Temporal evolution of energy transfer (*A*) and particle size (*B*) of equimolar mixtures of POPC/cholesterol/NBD-PE and POPC/cholesterol/rhodamine-DHPE at room temperature in the presence (●) and absence (○) of PP1.

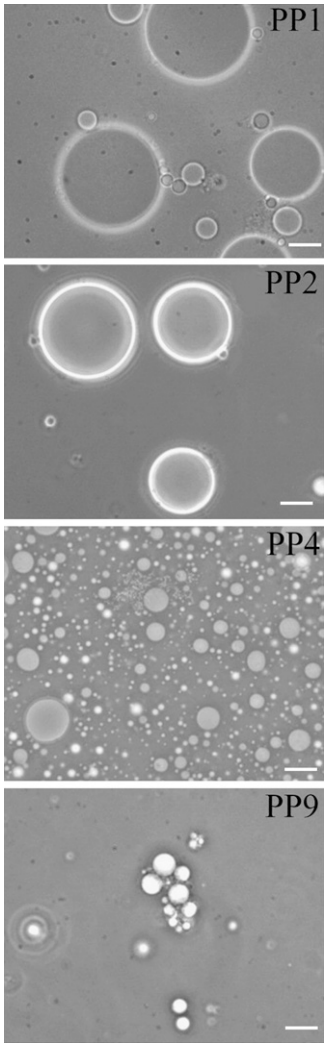

FIGURE 7 Phase-contrast microscopy shows that exposure of cholesterol (30 mol %)/POPC (70 mol %) unilamellar vesicles (~200 nm at time zero) to PP1 and PP2, both of which are high vapor pressure PFCs, for 72 h results in giant spherical vesicles of sizes ~20–40 μm, probably because of vesicle fusion. Giant vesicles are far fewer and smaller when exposed to PP4 and PP9; both are low vapor pressure PFCs. Bar, 10 μm.

absence of PFCs) remained virtually unchanged throughout the entire experiment, indicating that the GP changes observed were attributable to PFCs, and not to the instability of Laurdan-probe molecules over time.

DISCUSSION

The particle-size change induced by PP1, PP2, PP4, and PP9 is dramatic. It would be interesting to link these data with the respective membrane-water partition coefficients of the PFCs, which, however, are unknown at present. The partition coefficient of PFCs into membranes is determined by the combination of vapor pressure and lipid solubility. Membrane lipid solubility of the chosen PFCs is also unknown. Therefore, our interpretation of the data focused on vapor pressure. The PFCs PP1, PP2, PP4, and PP9 cover a broad range of vapor pressures, and the vapor pressure has biological relevance, as mentioned earlier.

When cholesterol (30 mol %)/POPC vesicles are exposed to high vapor pressure PFCs such as PP1 and PP2, there is a dramatic increase in particle size from 186 nm to 350–500 nm in the first 2 h (Fig. 2). The vesicle-size increase is correlated with lipid-mixing (Fig. 6), which suggests that high vapor pressure PFCs induce vesicle coalescence or vesicle fusion from an early time of PFC exposure. The size increase cannot be attributed purely to vesicle-swelling, which may lead to ~5–73% increase in vesicle size (37,38), and not the 200–300% shown in Fig. 2. The rate of particle-size increase observed in POPC (Fig. 3) and cholesterol (30 mol %)/POPC (Fig. 2) vesicles is much faster than that observed for vesicles

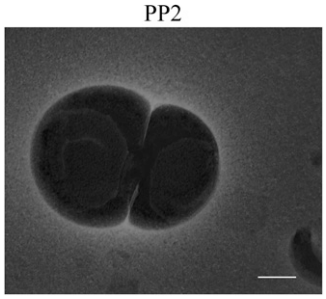

FIGURE 8 Negative-staining electron microscopy obtained from cholesterol (30 mol %)/POPC (70 mol %) after incubation with PP2 for 72 h. Image shows vesicle aggregation and coalescence. Bar, 200 nm.

composed of cholesterol/POPC/dye (NBD-PE or rhodamine-DHPE) (Fig. 6). This difference may be attributed to the repulsive interactions between vesicles carrying these fluorescent probes. At neutral pH, both NBD-PE and rhodamine-DHPE have a negative net charge that hinders vesicle aggregation, and subsequent vesicle coalescence and fusion. Nevertheless, the general trend that high vapor pressure PFCs induce vesicle coalescence or vesicle fusion,, and thus a dramatic increase in particle size, holds true for all the lipid vesicles investigated.

Fig. 2 also shows that high vapor pressure PFCs (i.e., PP1 and PP2) behave very differently from low vapor pressure PFCs (i.e., PP4 and PP9) in terms of changing vesicle sizes. It is likely that low vapor pressure PFCs do not induce vesicle aggregation as much as do high vapor pressure PFCs. Vesicle aggregation is a prerequisite of vesicle coalescence and fusion. Many studies showed that vesicle aggregation is often followed by vesicle fusion (31,39). In this study, our EM and phase-contrast microscopy data (Figs. 7 and 8), as well as energy-transfer studies (Figs. 5 and 6 *A*), suggest extensive lipid-mixing and massive vesicle fusion after incubation with PP1 and PP2. In comparison, low vapor pressure PFCs (PP4 and PP9) produced much less vesicle fusion (Fig. 7). Aggregation is known to be promoted by lipid polar headgroup dehydration (40). Elevated hydrostatic pressure is able to reduce lipid headgroup water content, according to Czeslik

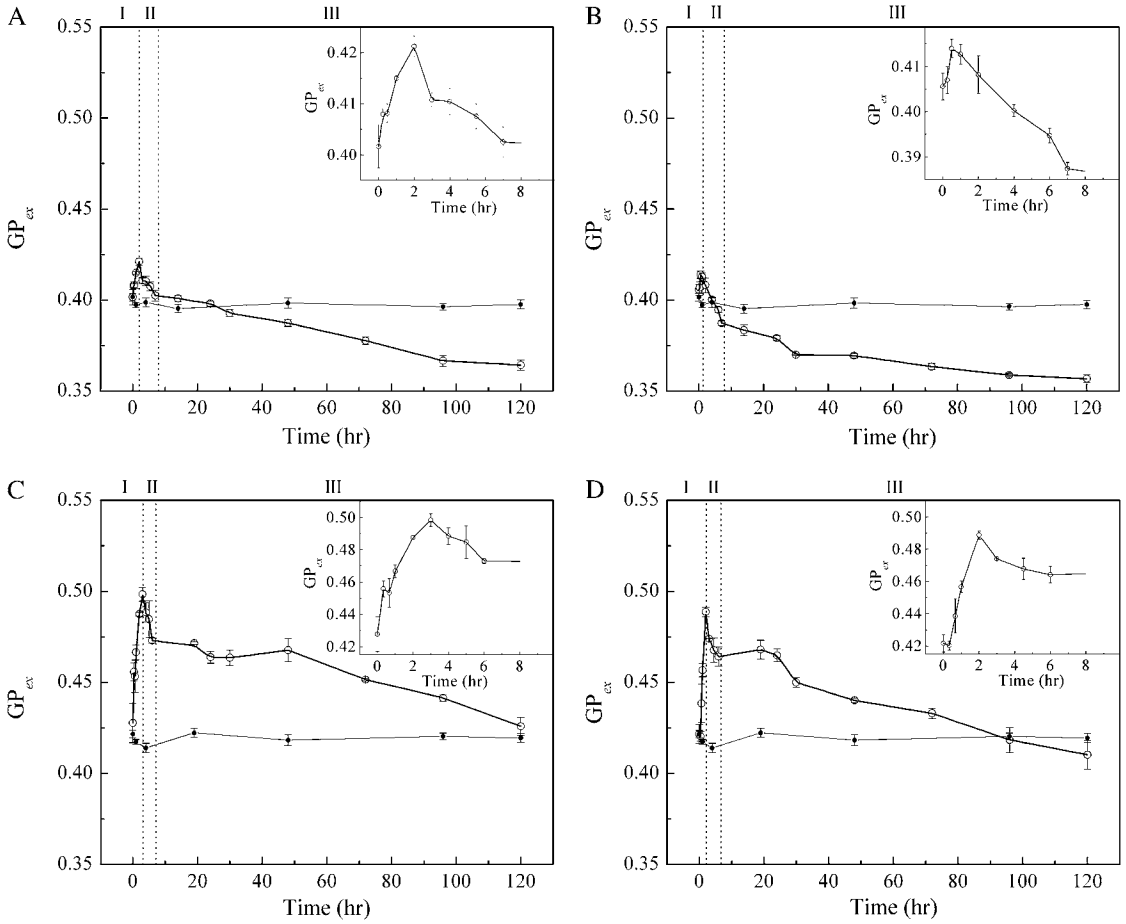

FIGURE 9 Temporal evolution of Laurdan's generalized polarization (GP) of POPC/cholesterol vesicles in the presence of (*A*) PP1, (*B*) PP2, (*C*) PP4, and (*D*) PP9. Open circles indicate vesicles incubated with PFC; solid circles indicate vesicles in absence of PFCs. (*Insets*) Details of first 8 h of GP profile. Three different stages described in text are indicated as I, II, and III.

et al. (41). Although the hydrostatic pressure range used in the study of Czeslik et al. (41) was 3–4 orders of magnitude higher than the vapor pressure dealt with in this study, it is still possible that the high vapor pressures possessed by PP1 and PP2 promote headgroup dehydration, and as a result produce more vesicle aggregation than the low vapor pressures of PP4 and PP9. The vapor pressure generates an osmotic pressure because of differences in solute concentration inside and outside the membrane. Thus, the force applied to the membrane because of osmotic pressure is directional. In contrast, the hydrostatic pressure experienced by a membrane is nondirectional.

Another factor contributing to massive vesicle fusion is the high PFC concentration gradient across the membrane. Because PFC liquids are immiscible with water and have a higher density than water, they remain at the bottom of the vial, surrounded by the aqueous suspensions of vesicles. In the experimental setting used here, PFC molecules can migrate from liquid droplets through the aqueous phase into the gas phase. In equilibrium, a constant amount of PFC molecules in the gas phase will create the vapor pressure and a constant rate of exchange of PFC molecules across the PFC liquid-water, water-gaseous phase, and water-membrane interfaces. The hydrophobic nature of PFC molecules allows them to partition into lipid membranes, and possibly migrate into the vesicle lumen. When the sample is exposed to higher vapor pressure PFC liquids (e.g., PP1 and PP2), more individual PFC molecules can enter the aqueous phase from PFC liquid droplets or from the gaseous phase. This will generate a high PFC concentration gradient across the vesicular membrane, which may cause microdomain sinking (42) or vesicle-swelling (43,44).

Microdomain sinking was directly visualized by fluorescence microscopy on membranes that were under a chemical or mechanical stress such as a large concentration gradient across the membrane (42). Microdomains are known to exist in our cholesterol-containing samples (Figs. 2, and 4–8). When subject to a high PFC concentration gradient, the interfacial regions between the highly ordered lipid microdomains (e.g., sterol superlattices (20) or lipid rafts (45)) and the rather disordered bulk domains are frustrated, leading to microdomain sinking (or vesicular endocytosis) (42). Microdomains may also occur in cholesterol-free membranes in the presence of PFC liquids (Fig. 3). Perfluorocarbons are lipophilic, but they also tend to form liquid droplets. Therefore, after individual PFC molecules insert into lipid membranes, they may aggregate to form lateral domains in the membrane. These domains can, in principle, undergo domain sinking under a high PFC concentration gradient. This explains why high vapor pressure PFCs can also induce considerable changes in particle size in cholesterol-free POPC vesicles, although the rate of the size change is significantly slower (Fig. 3).

The data in Fig. 4 further suggest that the rate of PFC-induced particle-size increase varies with lipid-membrane domain size, i.e., the extent of sterol superlattice in the membrane. When the extent of sterol superlattice (superlattice domain) is small, which occurs at noncritical mole fractions such as 21.0 and 23.4 mol % sterol in POPC, the initial rate of particle-size change is relatively fast (Fig. 4). When the extent of sterol superlattice (superlattice domain) is large (~71–89% of the total surface area at critical sterol mole fractions, C_r) (46,47), the initial rate of particle-size change becomes relatively slow (22.2 mol % cholesterol, Fig. 4). These data (Fig. 4), taken together with the data shown in Fig. 3, suggest that when the domain does not exist (POPC only, Fig. 3) or is too big (22.2 mol % sterol, Fig. 4), high vapor pressure PFCs induce less vesicle fusion. When the domain exists but the domain size is moderate (in the cases of 21.0 and 23.4 mol % sterol in POPC, Fig. 4), high vapor pressure PFCs induce more dramatic vesicle fusion (Figs. 2 and 4), probably because of increased domain sinking.

Microdomain sinking (42) is likely to create transient membrane defects, through which membrane fusion starts (42). Cell studies showed that PFCs can enter the cytoplasm and form vacuole-like particles (48,49). Those particles may be associated with internalized membranes with entrapped PFC liquids. The EM picture in Fig. 8 displays internal vesicular structures in opposing vesicles; this seems to be in good agreement with our domain-sinking hypothesis.

The presence of small amounts of NBD-PE and rhodamine-DHPE, both of which possess bulky polar headgroups, may attenuate the formation of cholesterol-related liquid-ordered domains such as sterol superlattices (20,28,29). It is then possible that PP1-induced domain-sinking is less in the mixture of POPC/cholesterol/NBD-PE and POPC/cholesterol/rhodamine-DHPE than in cholesterol (30 mol %)/POPC bilayers. This, in addition to the surface charge mentioned earlier, also explains why the PP1-induced particle-size change in this particular mixture (Fig. 6 *B*) is less dramatic than in the mixture of cholesterol (30 mol %) and POPC (Fig. 2 *A*).

Vesicle-swelling is also known to induce vesicle fusion (38,43,44). However, the data in Fig. 3 seem to argue against this possibility. Vesicle-swelling is supposed to be more difficult in cholesterol-containing PC vesicles than in pure PC bilayers, because cholesterol is known to stabilize (condense) fluid lipid bilayers. In this sense, the data in Fig. 3 (*inset*) do not support the vesicle-swelling hypothesis, but do agree with the domain-sinking model. Microdomains are supposed to be more abundant in cholesterol-containing PC vesicles than in pure PC bilayers. Our data show that the initial rate of the PP1-induced or PP2-induced particle-size increase with time is less for POPC than for POPC-cholesterol (molar ratio, 7:3) mixtures (Fig. 3, *inset*).

Another factor contributing to vesicle fusion could be the possible high level of PFC partitioning into lipid vesicles in the cases of PP1 and PP2. The insertion of PFC may disrupt membrane packing, which creates local membrane defects and leads to vesicle fusion (42).

Molecular events such as vesicle aggregation, swelling, domain-sinking, and vesicle fusion can be used to explain the GP data (Fig. 9). There is an initial increase in GP in region I for all PFCs examined (Fig. 8). This initial increase in GP is likely attributable to vesicle aggregation, which is usually accompanied by headgroup dehydration. When the water level near the lipid polar headgroup regions is reduced, the GP value becomes high (21). The subsequent steady decrease in GP with time (Fig. 9, *regions II* and *III*) may be attributable to a gradual disruption of membrane structure as a result of domain-sinking or vesicle-swelling or PFC insertion, as well as vesicle fusion. When exposed to high vapor pressure PFCs such as PP1 and PP2, the initial increase in GP in cholesterol/POPC mixtures is less than that observed from low vapor pressure studies. A possible explanation is that, when exposed to PP1 and PP2, a large number of small vesicles aggregate. Moreover, when vesicle aggregation occurs, domain-sinking or vesicle-swelling will also begin. The former increases GP, whereas the latter decreases GP. Because of these opposite effects, the initial GP increase attributable to PP1 and PP2 is less, compared with PP4 and PP9.

When exposed to PP4 and PP9 (low vapor pressures), vesicle aggregation may also occur, but the aggregates may involve a smaller number of original vesicles. Thus, particle size does not increase much in region I (Fig. 2). However, this limited vesicle aggregation still leads to vesicle fusion, although to a much lower extent, as evidenced by the data in Figs. 2 and 7. In this case, aggregation itself gives rise to an increase in GP, but the opposite effect on GP attributable to domain-sinking, vesicle-swelling, and vesicle fusion is relatively little. As a result, there is a larger initial increase in GP (Fig. 9, region *I*) for PP4 and PP9.

The origin of the antiinflammatory effect of PFCs is unclear. Perfluorocarbons do not affect direct binding between the ligand (e.g., concanavalin A) and the receptor (e.g., mannosylated glycoprotein) (50). Woods et al. reported that the diffusion of perflubron (a PFC) from the alveolar space into the pulmonary vascular endothelial layer may modulate neutrophil adhesion, and thereby reduce the rate of infiltration of activated neutrophils into the injured lung (26). Chang et al. suggested that FC-77 (a PFC) inhibits inflammatory responses in lipopolysaccharide-stimulated macrophages by attenuating the nuclear factor NF-κB-dependent induction of the cyclooxygenase-2/prostaglandin E_2 pathway and the proinflammatory/antiinflammatory cytokine ratio (51). Haeberle et al. reported that treatment with perflubron abrogated NF-κB activation in the lungs of respiratory syncytial virus-infected mice (13). Nuclear factor NF-κB is a protein controlling the gene expression of proinflammatory mediators (52). Because it is known that the activation of NF-κB can be affected by membrane proteins and lipids (53, 54) and by surface active agents such as detergents and anesthetics (55), it is logical to suggest that PFCs cause marked changes in membrane fusion and membrane packing, as revealed in this study, which in turn cause changes in the activation of NF-κB, thus inducing antiinflammatory responses. A few other studies also proposed that PFCs perturb the cell membrane, subsequently altering intracellular signal-transduction pathways (15,48,50,56–58). Perfluorocarbons influence the release and expression of proinflammatory mediators in a nonspecific manner, in accordance with the idea that the effects of PFCs involve cell-membrane modification (15,50).

As shown in Fig. 7, exposure of vesicles to high vapor pressure PFCs can lead to giant vesicles of 20–40 μm. This represents a new way, we believe, to generate giant vesicles for microscopy studies. Whether the PFC-induced giant vesicles are unilamellar or not is yet to be determined.

In conclusion, our results show for the first time, to our knowledge, that high vapor pressure PFCs have strong fusogenic activity with lipid vesicles, particularly those with moderate lipid microdomains, and can produce marked changes in membrane packing in a time-dependent manner. These results may help elucidate the molecular mechanisms of PFC-membrane interactions in cells. This level of understanding may improve the use and development of biomedical applications of PFCs (see Introduction), and will prove helpful in choosing appropriate PFC physiochemical properties to rationalize the design of PFC treatments.

We are thankful for support from the American Heart Association (P.L.-G.C.: grant 0255082N), the Pennsylvania Department of Health (P.L.-G.C., M.R.W.), and the National Science Foundation (P.L.-G.C.: DMR-0706410).

REFERENCES

1. Krafft, M. P. 2001. Fluorocarbons and fluorinated amphiphiles in drug delivery and biomedical research. *Adv. Drug Deliv. Rev.* 47:209–228.
2. Greenspan, J. S., M. R. Wolfson, S. D. Rubenstein, and T. H. Shaffer. 1990. Liquid ventilation of human preterm neonates. *J. Pediatr.* 117:106–111.
3. Stavis, R. L., M. R. Wolfson, C. Cox, N. Kechner, and T. H. Shaffer. 1998. Physiologic, biochemical, and histologic correlates associated with tidal liquid ventilation. *Pediatr. Res.* 43:132–138.
4. Wolfson, M. R., and T. H. Shaffer. 2005. Pulmonary applications of perfluorochemical liquids: ventilation and beyond. *Paediatr. Respir. Rev.* 6:117–127.
5. Wolfson, M. R., J. S. Greenspan, and T. H. Shaffer. 1996. Pulmonary administration of vasoactive substances by perfluorochemical liquid ventilation in neonatal lambs. *Pediatrics.* 97:449–455.
6. Yamanouchi, K., M. Tanaka, Y. Tsuda, K. Yokoyama, S. Awazu, and Y. Kobayashi. 1985. Quantitative structure-*in vivo* half-life relationships of perfluorochemicals for use as oxygen transporters. *Chem. Pharm. Bull. (Tokyo).* 33:1221–1231.
7. Gross, U., S. Rüdiger, and H. Reichelt. 1991. Perfluorocarbons: chemically inert but biologically active? *J. Fluor. Chem.* 53:155–161.
8. Gale, S. C., G. D. Gorman, J. G. Copeland, and P. F. McDonagh. 2007. Perflubron emulsion prevents PMN activation and improves myocardial functional recovery after cold ischemia and reperfusion. *J. Surg. Res.* 138:135–140.
9. Lehmler, H. 2007. Perfluorocarbon compounds as vehicles for pulmonary drug delivery. *Expert. Opin. Drug Deliv.* 4:247–262.
10. Wolfson, M. R., R. G. Stern, N. Kechner, K. M. Sekins, and T. H. Shaffer. 1994. Utility of a perfluorochemical liquid for pulmonary

diagnostic imaging. *Artif. Cells Blood Substit. Immobil. Biotechnol.* 22:1409–1420.

11. Winter, P. M., K. Cai, S. D. Caruthers, S. A. Wickline, and G. M. Lanza. 2007. Emerging nanomedicine opportunities with perfluorocarbon nanoparticles. *Expert Rev. Med. Devices.* 4:137–145.
12. Holscher, T., J. A. Sattin, R. Raman, W. Wilkening, C. V. Fanale, S. E. Olson, R. F. Mattrey, and P. D. Lyden. 2007. Real-time cerebral angiography: sensitivity of a new contrast-specific ultrasound technique. *AJNR* 28:635–639.
13. Haeberle, H. A., F. Nesti, H. J. Dieterich, Z. Gatalica, and R. P. Garofalo. 2002. Perflubron reduces lung inflammation in respiratory syncytial virus infection by inhibiting chemokine expression and nuclear factor-kappa B activation. *Am. J. Respir. Crit. Care Med.* 165:1433–1438.
14. Shashikant, B. N., T. L. Miller, M. J. Jeng, J. Davis, T. H. Shaffer, and M. R. Wolfson. 2005. Differential impact of perfluorochemical physical properties on the physiologic, histologic, and inflammatory profile in acute lung injury. *Crit. Care Med.* 33:1096–1103.
15. Obraztsov, V. V., G. G. Neslund, E. S. Kornbrust, S. F. Flaim, and C. M. Woods. 2000. *In vitro* cellular effects of perfluorochemicals correlate with their lipid solubility. *Am. J. Physiol. Lung Cell. Mol. Physiol.* 278:L1018–L1024.
16. Ellena, J. F., V. V. Obraztsov, V. L. Cumbea, C. M. Woods, and D. S. Cafiso. 2002. Perfluorooctyl bromide has limited membrane solubility and is located at the bilayer center: locating small molecules in lipid bilayers through paramagnetic enhancements of NMR relaxation. *J. Med. Chem.* 45:5534–5542.
17. Gerber, F., M. P. Krafft, T. F. Vandamme, M. Goldmann, and P. Fontaine. 2006. Fluidization of a dipalmitoyl phosphatidylcholine monolayer by fluorocarbon gases: potential use in lung surfactant therapy. *Biophys. J.* 90:3184–3192.
18. Jeng, M. J., S. S. Yang, B. Hwang, M. R. Wolfson, and T. H. Shaffer. 2006. Effects of perfluorochemical evaporative properties on oxygenation during partial liquid ventilation. *Pediatr. Int.* 48:608–615.
19. Hope, M. J., M. B. Bally, G. Webb, and P. R. Cullis. 1985. Production of large unilamellar vesicles by a rapid extrusion procedure. Characterization of size distribution, trapped volume and ability to maintain a membrane potential. *Biochim. Biophys. Acta.* 812:55–65.
20. Venegas, B., I. P. Sugar, and P. L.-G. Chong. 2007. Critical factors for detection of biphasic changes in membrane properties at specific sterol mole fractions for maximal superlattice formation. *J. Phys. Chem. B.* 111:5180–5192.
21. Parasassi, T. G., and E. Gratton. 1995. Membrane lipid domains and dynamics as detected by Laurdan fluorescence. *J. Fluoresc.* 5:59–69.
22. Chong, P. L.-G., and P. T. T. Wong. 1993. Interactions of Laurdan with phosphatidylcholine liposomes: a high pressure FTIR study. *Biochim. Biophys. Acta.* 1149:260–266.
23. Zeng, J., and P. L.-G. Chong. 1995. Effect of ethanol-induced lipid interdigitation on the membrane solubility of prodan, acdan, and Laurdan. *Biophys. J.* 68:567–573.
24. Bagatolli, L. A., and E. Gratton. 2000. Two photon fluorescence microscopy of coexisting lipid domains in giant unilamellar vesicles of binary phospholipid mixtures. *Biophys. J.* 78:290–305.
25. Brown, D. 2006. Biophysical properties and applications of archaeosomes. MS Thesis, Temple University School of Medicine, Philadelphia, PA.
26. Woods, C. M., G. Neslund, E. Kornbrust, and S. F. Flaim. 2000. Perflubron attenuates neutrophil adhesion to activated endothelial cells *in vitro*. *Am. J. Physiol. Lung. Cell. Mol. Physiol.* 278:L1008–L1017.
27. Chong, P. L.-G., and M. Olsher. 2004. Fluorescence studies of the existence and functional importance of regular distributions in liposomal membranes. *Soft Materials.* 2:85–108.
28. Chong, P. L.-G. 1994. Evidence for regular distribution of sterols in liquid crystalline phosphatidylcholine bilayers. *Proc. Natl. Acad. Sci. USA.* 91:10069–10073.
29. Virtanen, J. A., M. Ruonala, M. Vauhkonen, and P. Somerharju. 1995. Lateral organization of liquid-crystalline cholesterol-dimyristoylphosphatidylcholine bilayers: evidence for domains with hexagonal and centered rectangular cholesterol superlattices. *Biochemistry.* 34:11568–11581.
30. Liu, F., I. P. Sugar, and P. L.-G. Chong. 1997. Cholesterol and ergosterol superlattices in three-component liquid crystalline lipid bilayers as revealed by dehydroergosterol fluorescence. *Biophys. J.* 72: 2243–2254.
31. Wong, M., and T. E. Thompson. 1982. Aggregation of dipalmitoylphosphatidylcholine vesicles. *Biochemistry.* 21:4133–4139.
32. Arnold, K., and K. Gawrisch. 1993. Effects of fusogenic agents on membrane hydration: a deuterium nuclear magnetic resonance approach. *Methods Enzymol.* 220:143–157.
33. Bagatolli, L. A., E. Gratton, and G. D. Fidelio. 1998. Water dynamics in glycosphingolipid aggregates studied by Laurdan fluorescence. *Biophys. J.* 75:331–341.
34. Parasassi, T., G. De Stasio, G. Ravagnan, R. M. Rusch, and E. Gratton. 1991. Quantitation of lipid phases in phospholipid vesicles by the generalized polarization of Laurdan fluorescence. *Biophys. J.* 60:179–189.
35. Bagatolli, L. A., E. Gratton, T. K. Khan, and P. L.-G. Chong. 2000. Two-photon fluorescence microscopy studies of bipolar tetraether giant liposomes from thermoacidophilic archaebacteria *Sulfolobus acidocaldarius*. *Biophys. J.* 79:416–425.
36. Parasassi, T. G., E. Krasnowska, and L. A. Bagatolli. 1998. Laurdan and prodan as polarity-sensitive fluorescent membrane probes. *J. Fluoresc.* 8:365–373.
37. Ertel, A., A. G. Marangoni, J. Marsh, F. R. Hallett, and J. M. Wood. 1993. Mechanical properties of vesicles. I. Coordinated analyses of osmotic swelling and lysis. *Biophys. J.* 64:426–434.
38. Brodwick, M. S., M. Curran, and C. Edwards. 1992. Effects of osmotic stress on mast cell vesicles of the beige mouse. *J. Membr. Biol.* 126:159–169.
39. Wilschut, J., S. Nir, J. Scholma, and D. Hoekstra. 1985. Kinetics of Ca^{2+}-induced fusion of cardiolipin-phosphatidylcholine vesicles: correlation between vesicle aggregation, bilayer destabilization and fusion. *Biochemistry.* 24:4630–4636.
40. Minami, H., and T. Inoue. 1999. Aggregation of dipalmitoylphosphatidylcholine vesicles induced by some metal ions with high activity for hydrolysis. *Langmuir.* 15:6643–6651.
41. Czeslik, C., O. Reis, R. Winter, and G. Rapp. 1998. Effect of high pressure on the structure of dipalmitoylphosphatidylcholine bilayer membranes: a synchrotron-x-ray diffraction and FT-IR spectroscopy study using the diamond anvil technique. *Chem. Phys. Lipids.* 91:135–144.
42. Hamada, T., Y. Miura, K. Ishii, S. Araki, K. Yoshikawa, M. Vestergaad, and M. Takagi. 2007. Dynamic processes in endocytic transformation of raft-exhibiting giant liposomes. *J. Phys. Chem. B.* 111:10853–10857.
43. Cohen, F. S., M. H. Akabas, and A. Finkelstein. 1982. Osmotic swelling of phospholipid vesicles causes them to fuse with a planar phospholipid bilayer membrane. *Science.* 217:458–460.
44. Malinin, V. S., P. Frederik, and B. R. Lentz. 2002. Osmotic and curvature stress affect PEG-induced fusion of lipid vesicles but not mixing of their lipids. *Biophys. J.* 82:2090–2100.
45. Kusumi, A., I. Koyama-Honda, and K. Suzuki. 2004. Molecular dynamics and interactions for creation of stimulation-induced stabilized rafts from small unstable steady-state rafts. *Traffic.* 5:213–230.
46. Wang, M. M., I. P. Sugar, and P. L.-G. Chong. 1998. Role of the sterol superlattice in the partitioning of the antifungal drug nystatin into lipid membranes. *Biochemistry.* 37:11797–11805.
47. Wang, M. M., M. Olsher, I. P. Sugar, and P. L.-G. Chong. 2004. Cholesterol superlattice modulates the activity of cholesterol oxidase in lipid membranes. *Biochemistry.* 43:2159–2166.
48. Koch, T., M. Ragaller, D. Haufe, A. Hofer, M. Grosser, D. M. Albrecht, M. Kotzsch, and T. Luther. 2001. Perfluorohexane attenuates proinflammatory and procoagulatory response of activated monocytes and alveolar macrophages. *Anesthesiology.* 94:101–109.
49. Nakstad, B., M. R. Wolfson, T. H. Shaffer, H. Kahler, R. Lindemann, D. Fugelseth, and T. Lyberg. 2001. Perfluorochemical liquids modulate

cell-mediated inflammatory responses. *Crit. Care Med.* 29:1731–1737.

50. Haufe, D., T. Luther, M. Kotzsch, L. Knels, and T. Koch. 2004. Perfluorocarbon attenuates response of concanavalin A-stimulated mononuclear blood cells without altering ligand-receptor interaction. *Am. J. Physiol. Lung Cell. Mol. Physiol.* 287:L210–L216.
51. Chang, H., F. C. Kuo, Y. S. Lai, and T. C. Chou. 2005. Inhibition of inflammatory responses by FC-77, a perfluorochemical, in lipopolysaccharide-treated RAW 264.7 macrophages. *Intensive Care Med.* 31:977–984.
52. Mackman, N. 1995. Regulation of the tissue factor gene. *FASEB J.* 9: 883–889.
53. Signorelli, P., C. Luberto, and Y. A. Hannun. 2001. Ceramide inhibition of NF-kappa B activation involves reverse translocation of classical protein kinase C (PKC) isoenzymes: requirement for kinase activity and carboxyl-terminal phosphorylation of PKC for the ceramide response. *FASEB J.* 15:2401–2414.
54. Vile, G. F., A. Tanew-Ilitschew, and R. M. Tyrrell. 1995. Activation of NF-kappa B in human skin fibroblasts by the oxidative stress generated by UVA radiation. *Photochem. Photobiol.* 62:463–468.
55. Thomassen, M. J., J. M. Antal, B. P. Barna, L. T. Divis, D. P. Meeker, and H. P. Wiedemann. 1996. Surfactant downregulates synthesis of DNA and inflammatory mediators in normal human lung fibroblasts. *Am. J. Physiol.* 270:L159–L163.
56. Steinhorn, D. M., C. L. Leach, B. P. Fuhrman, and B. A. Holm. 1996. Partial liquid ventilation enhances surfactant phospholipid production. *Crit. Care Med.* 24:1252–1256.
57. Thomassen, M. J., L. T. Buhrow, and H. P. Wiedemann. 1997. Perflubron decreases inflammatory cytokine production by human alveolar macrophages. *Crit. Care Med.* 25:2045–2047.
58. Fernandez, R., V. Sarma, E. Younkin, R. B. Hirschl, P. A. Ward, and J. G. Younger. 2001. Exposure to perflubron is associated with decreased Syk phosphorylation in human neutrophils. *J. Appl. Physiol.* 91:1941–1947.